A Study on Guidance Technique for Precise Lunar Landing

By Satoshi Ueda,[1)] Takahiro Ito,[1)] and Shin-ichiro Sakai[1)]

[1)]*Institute of Space and Astronautical Science, JAXA, Sagamihara, Japan*

After JAXA's SELENE mission and NASA's LRO mission, precise pictures of lunar surface were obtained, and science communities are encouraged to propose exploration missions that target specific landing point. Those missions require precise landing technique. Traditional ways of guidance, navigation and control may not achieve this objective because of limitation of orbital determination accuracy, geographical error of lunar surface map, and short time landing sequence. To overcome these problems, autonomous guidance logic that robustly targets the landing point is required, because short time landing sequence does not allow real-time flight plan update from the ground station. This study focuses on autonomous guidance logic for precise lunar landing. In this paper, the concept of the guidance logic that derives solution even in the condition with navigation errors and control errors is introduced, followed by its consideration of robustness and accuracy with simulation results.

Key Words: GN&C, Lunar Landing, Accuracy, Robustness

Nomenclature

t	:	time
$\boldsymbol{r}$	:	position vector wrt. center of the moon
$\boldsymbol{v}$	:	velocity vector wrt. center of the moon
m	:	total mass of the spacecraft
F	:	thruster force for trajectory control
β	:	downrange angle
ε	:	crossrange angle
r	:	orbit radius
ϕ	:	attitude angle (roll)
θ	:	attitude angle (pitch)
ψ	:	attitude angle (yaw)
μ_{moon}	:	the gravitational constant times the mass of the moon
R_{moon}	:	radius of the moon
g_e	:	standard gravity
I_{SP}	:	specific impulse
f_0	:	coefficient of F-m fitting curve
f_1	:	coefficient of F-m fitting curve
f_2	:	coefficient of F-m fitting curve
X, Y, Z	:	axes of inertial frame
e_x	:	unit vector parallel to X axis
e_y	:	unit vector parallel to Y axis
e_z	:	unit vector parallel to Z axis
e_β	:	unit vector of local frame
e_ε	:	unit vector of local frame
e_r	:	unit vector of local frame
v_β	:	velocity component
v_ε	:	velocity component
v_r	:	velocity component
DR	:	Downrange
CR	:	Crossrange
h	:	altitude
T	:	duration of guidance
$\boldsymbol{X}$	:	states of trajectory
τ	:	non-dimensional time
α	:	non-dimensional coefficient
a, b, c	:	polynomial coefficients
τ_f	:	end condition of non-dimensional time
D, P	:	intermediate variables of guidance logic

Subscripts

b	:	boosting section
c	:	coasting section
i	:	step number
end	:	end of steps
ini	:	initial condition
$term$	:	end condition

1. Introduction

Concerning previous lunar landing missions in the history, their landing strategies were to land safely to any place in widely dispersed landing area. After JAXA's SELENE mission and NASA's LRO mission, precise pictures of lunar surface were obtained, and science communities are encouraged to propose exploration missions that target specific landing point. Those missions require precise landing technique that enables the lander to be landed next to specific "scientifically attractive rock" safely. [1-5)]

Traditional ways of guidance, navigation and control may not achieve this objective because of limitation of orbital determination accuracy, geographical error of lunar surface map, and short time landing sequence. To overcome these problems, autonomous navigation based on terrain pictures obtained by on-board camera is required, because it directly estimates relative states to aimed landing point. [6, 7)] Autonomous guidance logic that robustly targets the landing

point is also required, because short time landing sequence does not allow real-time flight plan update from the ground station.

This study focuses on autonomous guidance logic for precise lunar landing. First, as usually considered in general space mission development, an optimal nominal trajectory in terms of minimum fuel consumption is investigated. Second, a guidance logic that derives guidance solution close to nominal trajectory based on on-board navigation solution even in the condition with navigation errors and control errors is developed. Third, the guidance logic is verified by means of simulation.

In this paper, the concept of the guidance logic and its practical solution example is introduced, followed by its consideration of robustness and accuracy with simulation results.

2. Landing Sequence

This study targets JAXA's small lunar landing demonstrator "SLIM" mission for achieving precise lunar landing. Figure 1 shows conceptual explanation of trajectory design of lunar circular orbit and descending trajectory. After separated from launcher, the spacecraft is inserted into lunar polar circular orbit. The spacecraft stays in the circular orbit for several weeks until the orbital plane crosses the landing target point. Once the condition is met, the spacecraft performs landing sequence as follow. First, the spacecraft performs descending orbital maneuver to decrease perilune altitude. Second, at the perilune point, the spacecraft starts powered descending to reduce its horizontal velocity. Third, after completion of powered descending, the spacecraft reduces remaining vertical velocity in parallel with guidance error correction and obstacle avoidance. These three phases are named as 'lunar orbit phase', 'powered descending phase', and 'vertical descending phase'. The guidance logic discussed in this study focuses on the guidance logic for powered descending phase.

During powered descending phase, coasting section is introduced to perform attitude maneuver for pointing of body-fixed navigation camera. During coasting sections, the spacecraft executes vision based navigation according to obtained pictures of the moon surface. IMU navigation is initialized according to the result of vision based navigation, then the spacecraft performs guidance update for next boosting section with updated IMU navigation. Figure 2 shows conceptual explanation of guidance and navigation update sequence during powered descending phase. During coasting section, the spacecraft stops main thruster burn for attitude maneuver that leads to the condition of no trajectory control force. Therefore, coasting effect must be taken into consideration as a design conditions for nominal powered descending trajectory.

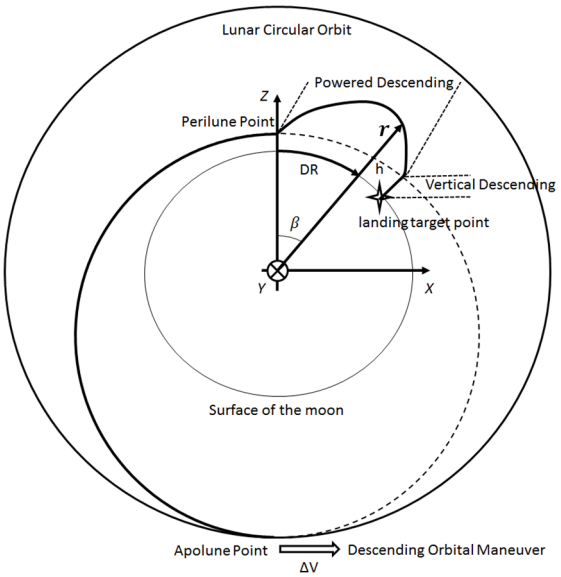

Fig. 1. Conceptual explanation of trajectory design.

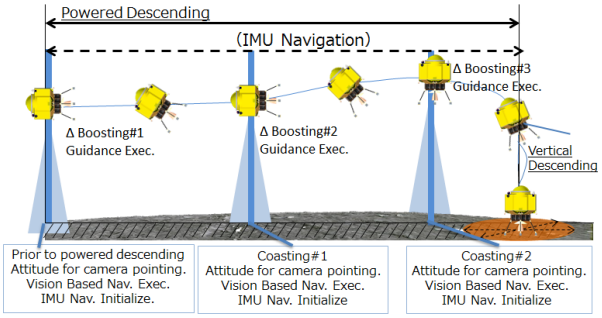

Fig. 2. Conceptual explanation of guidance and navigation update sequence during powered descending phase.

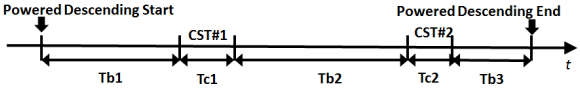

Fig. 3. Definition of duration of boosting sections and coasting sections.

Duration of boosting sections and coasting sections are defined as shown in Fig. 3. The duration of each section is design parameter of nominal powered descending trajectory, e.g., the longer duration of coasting section may provide additional chance of obtaining pictures for vision based navigation but it leads to increase of gravity loss.

3. Nominal Trajectory Design

3.1. Equations of motion

Nominal trajectory for powered descending phase is derived based on optimization technique. Formulation of the optimization problem assumes that the trajectory is constrained in the orbital plane, therefore crossrange component is assumed to be zero for trajectory design purpose. The equations of motion applied to this purpose is introduced as follows.

$$\dot{\boldsymbol{r}} = \boldsymbol{v} \tag{1}$$

$$\dot{\boldsymbol{v}} = -\frac{\mu_{moon}}{\boldsymbol{r}\cdot\boldsymbol{r}}\frac{\boldsymbol{r}}{\|\boldsymbol{r}\|} + \frac{F}{m}(\sin(\beta+\theta)\cdot\boldsymbol{e_x} + \cos(\beta+\theta)\cdot\boldsymbol{e_z}) \tag{2}$$

$$\dot{m} = -\frac{F}{g_e \cdot I_{SP}} \tag{3}$$

where downrange angle β is defined by Eq. (4).

$$\beta = \tan^{-1}\left(\frac{\boldsymbol{r}\cdot\boldsymbol{e}_x}{\boldsymbol{r}\cdot\boldsymbol{e}_z}\right) \quad (4)$$

thruster force for trajectory control F is expressed as quadratic fitting function of total mass of the spacecraft m as shown in Eq. (5).

$$F = f_2 m^2 + f_1 m + f_0 \quad (5)$$

where coefficients of F-m fitting curve f_0, f_1, f_2 are predetermined values according to propellant tank pressure and total mass prediction at the beginning of powered descending phase. Geometric relation of trajectory design parameters is explained in Fig. 4. Applied constant values are shown in Table 1.

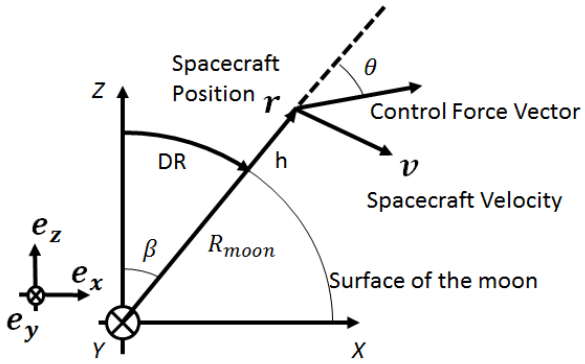

Fig. 4. Geometric relation of trajectory design parameters.

Table 1. Applied constant values.

Constants	Unit	Value
μ_{moon}	m^3/s^2	$4.902800222140800 \times 10^{12}$
g_e	m/s^2	9.80655
I_{SP}	s	304.3599207
R_{moon}	m	1738.0×10^3
f_0	N	3.94207309×10^2
f_1	N/kg	$1.99589120 \times 10^{-1}$
f_2	$N/(kg)^2$	$5.47454930 \times 10^{-4}$

3.2. Formulation of optimization problem

Nominal trajectory for powered descending phase is derived by solving optimization problem. The design parameters are selected as shown in Table 2.

Time series of states of trajectory and control input are divided into small steps. States are propagated according to Eqs. (1-5) within each step. Propagation results are expressed as Eq. (6).

$$\boldsymbol{X}_i^{prop} = A(\boldsymbol{X}_i, \theta_i) \quad (6)$$

where i denotes step number, $prop$ denotes propagated result. Equality constraints are formulated as shown in Eqs. (7-9) to express connection of continuing steps.

$$\boldsymbol{X}_1 = \boldsymbol{X}_{ini} \quad (7)$$

$$\boldsymbol{X}_{i+1} = \boldsymbol{X}_i^{prop} = A(\boldsymbol{X}_i, \theta_i) \text{ for all } i \quad (8)$$

$$\boldsymbol{X}_{term} = \boldsymbol{X}_{end}^{prop} = A(\boldsymbol{X}_{end}, \theta_{end}) \quad (9)$$

Table 2. Design parameters of trajectory optimization problem.

Design parameters	Definitions
$\boldsymbol{X}$	States of trajectory $\boldsymbol{X} = [\boldsymbol{r} \quad \boldsymbol{v} \quad m]$
θ	Control input (attitude angle pitch)
T_{b1}	Duration of 1st boosting section
T_{b2}	Duration of 2nd boosting section

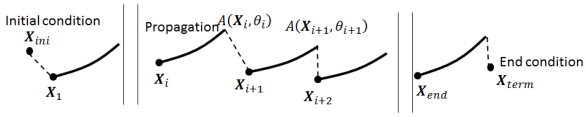

Fig. 5. Conceptual explanation of equality constraints to express connection of continuing steps.

Table 3. Boundary conditions of states of trajectory.

States	Unit	Initial Conditions	End Conditions
$\boldsymbol{r}$	m	$h = 15000$ $(\beta = 0)$	$h = 3500$
$\boldsymbol{v}$	m/s	$v_\beta = 1787.94$ $v_r = 0$	$v_\beta = 0$ $v_r = -40$
m	kg	Free	$m = 185$

Note: $v_\beta = \hat{\beta} r, \; v_r = \dot{r}$

Table 4. Objective function, constraints, and design parameters.

Items	Definitions	Design intention
Objective function	$\mathrm{J} = m_{t=0}$	Minimize fuel consumption.
Constraints	$T_{b1} = T_{b2}$	Equal duration of boosting#1 and boosting#2.
Design parameters	$T_{c1} = T_{c2} = 40s$ $T_{b3} = 200s$	Conditions derived from vision based navigation execution condition and IMU navigation accuracy.

where end denotes end of steps. Figure 5 shows conceptual explanation of equality constraints to express connection of continuing steps.

Boundary conditions of states of trajectory are shown in Table 3. The spacecraft starts powered descending at the perilune point whose altitude is 15 km. The end conditions are defined by considering interface conditions with vertical descending phase. In this study, end conditions are defined such that altitude is 3500 m and remaining vertical velocity is -40 m/s. Total mass of the spacecraft is fixed at the end of powered descending phase.

An objective function, constraints derived from design intention, and design parameters are listed in Table 4. An objective function is defined to minimize fuel consumption during powered descending phase. An equality constraint is set such that duration of boosting#1 is equal to that of boosting#2 for averaging accumulated error of IMU navigation. Design parameters regarding duration of coasting are derived from vision based navigation execution condition. Duration of boosting#3 is fixed by considering accumulated error of IMU navigation at the end of powered descending phase.

3.3. Optimization result

The optimization problem as defined in previous sections is

solved by SQP algorithm. A solution is shown in Table 5. Initial mass of the spacecraft is about 400 kg that means total fuel consumption during powered descending phase is about 215 kg. Shape of trajectory, time series of velocities, time series of control input (attitude pitch), and time series of total mass of the spacecraft are shown in Figs. 6-10.

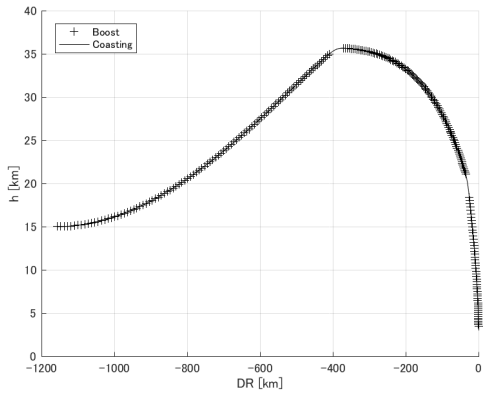

Fig. 6. Shape of trajectory (Downrange is expressed as distance from landing target point).

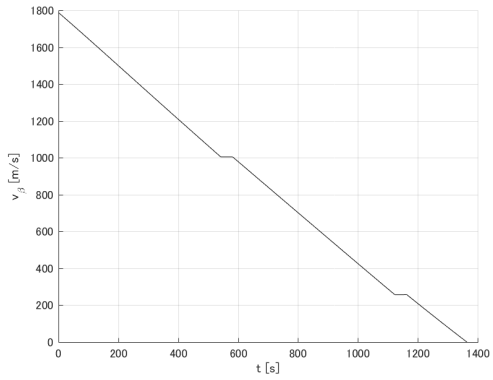

Fig. 7. Time series of horizontal velocity.

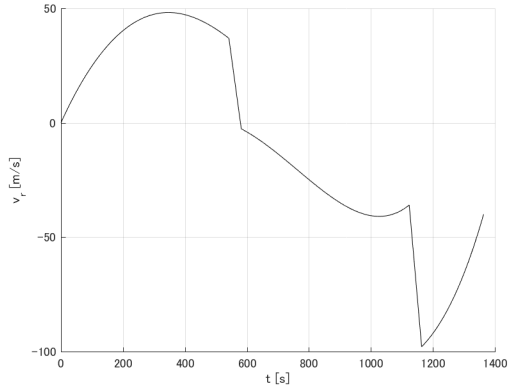

Fig. 8. Time series of vertical velocity.

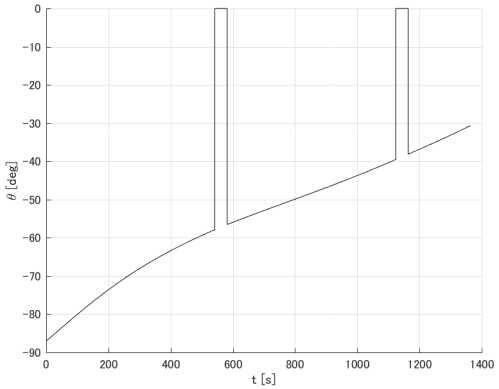

Fig. 9. Time series of control input (attitude pitch).

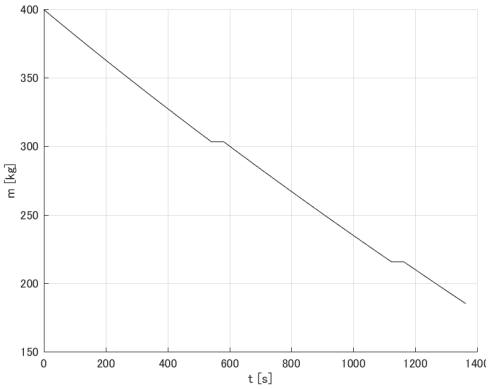

Fig. 10. Time series of total mass of the spacecraft.

Table 5. A solution of the optimization problem.

Items	Unit	Design result
Initial Mass $(m_{t=0})$	kg	399.79
Total flight time of powered descending phase $(T_{b1}+T_{c1}+T_{b2}+T_{c2}+T_{b3})$	s	1363.68
Duration of boosting#1 (T_{b1})	s	541.84
Duration of boosting#2 (T_{b2})	s	541.84
Total downrange	km	1156.76

4. Autonomous Guidance Logic

4.1. Equations of motion

Actual flight trajectory is deviated from the reference trajectory because of control error or navigation error, therefore the guidance logic is designed such that it autonomously incorporates on-board navigation solution then generates reference trajectory that must be followed by the spacecraft according to its on-board flight path tracking logic. Trajectory deviation is not only in-plane motion but also out-of-plane motion, therefore equation of motion applied to guidance logic must be 3-dimensional. Crossrange angle ε is introduced to express out-of-plane motion as explained in Fig. 11. Position vector $\boldsymbol{r}$ wrt. center of the moon is expressed as follows.

$$\boldsymbol{r} = r\ \cos\varepsilon\,\boldsymbol{e}_r + r\sin\varepsilon\,\boldsymbol{e}_\varepsilon \tag{10}$$

where $\boldsymbol{e}_\beta, \boldsymbol{e}_\varepsilon, \boldsymbol{e}_r$ denotes unit vectors of local frame those have mathematical relations as shown in Eqs. (11-13).

$$\dot{\boldsymbol{e}}_r = \dot{\beta}\boldsymbol{e}_\beta \tag{11}$$

$$\dot{\boldsymbol{e}}_\beta = -\dot{\beta}\boldsymbol{e}_r \tag{12}$$

$$\dot{\boldsymbol{e}}_\varepsilon = 0 \tag{13}$$

Second derivative of Eq. (10) derives equations of motion expressed in terms of β, ε, r as follows.

$$r\,\ddot{\beta} + 2\dot{r}\dot{\beta} = \frac{F_\beta}{m} \tag{14}$$

$$r\ddot{\varepsilon} + 2\dot{r}\dot{\varepsilon} = \frac{F_\varepsilon}{m} \tag{15}$$

$$\ddot{r} - r\left(\dot{\beta}^2 + \dot{\varepsilon}^2\right) = \frac{F_r}{m} - \frac{\mu_{moon}}{r^2} \tag{16}$$

where $F_\beta, F_\varepsilon, F_r$ denotes components of control force parallel to $\boldsymbol{e}_\beta, \boldsymbol{e}_\varepsilon, \boldsymbol{e}_r$ respectively.

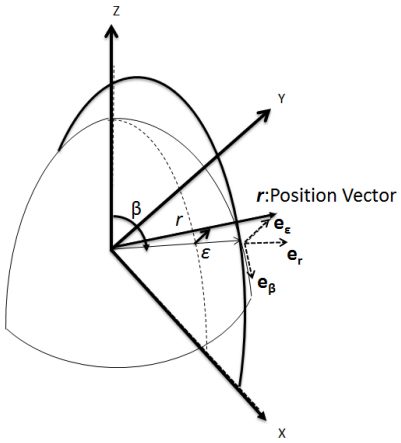

Fig. 11. Definition of crossrange angle ε.

4.2. Formulation of guidance logic

The guidance logic is based on 'Polynomial Guidance Law' that is presented in Refs. 1,4 and 5). In proposed guidance logic, β, ε, r are expressed as the function of non-dimensional time τ that is defined in Eq. (17).

$$t = \alpha(\tau)\tau \tag{17}$$

where $\alpha(\tau)$ denotes non-dimensional coefficient. α is calculated according to the constraint such that control force F must be equal to available force generated by thruster of the spacecraft.

The reference trajectory is expressed as shown in Eqs. (18-20).

$$\beta = a_0 + a_1\tau + a_2\tau^2 + a_3\tau^3 + a_4\tau^4 \tag{18}$$

$$\varepsilon = b_0 + b_1\tau + b_2\tau^2 + b_3\tau^3 \tag{19}$$

$$r = \frac{1}{c_0 + c_1\tau + c_2\tau^2 + c_3\tau^3 + c_4\tau^4} \tag{20}$$

where a, b, c denotes polynomial coefficients and their subscripts denote the order of coefficients.

Boundary conditions are reflected according to first and second derivatives of Eqs. (18-20).

$$\beta_{\tau=0} = \beta_{ini},\ \beta_{\tau=\tau_f} = \beta_{term} \tag{21}$$

$$\frac{d\beta}{d\tau}_{\tau=0} = \dot{\beta}_{ini},\ \frac{d\beta}{d\tau}_{\tau=\tau_f} = \dot{\beta}_{term}$$

$$\frac{d^2\beta}{d\tau^2}_{\tau=0} = \ddot{\beta}_{ini},\ \frac{d^2\beta}{d\tau^2}_{\tau=\tau_f} = \ddot{\beta}_{term}$$

$$\varepsilon_{\tau=0} = \varepsilon_{ini},\ \varepsilon_{\tau=\tau_f} = \varepsilon_{term} \tag{22}$$

$$\frac{d\varepsilon}{d\tau}_{\tau=0} = \dot{\varepsilon}_{ini},\ \frac{d\varepsilon}{d\tau}_{\tau=\tau_f} = \dot{\varepsilon}_{term}$$

$$r_{\tau=0} = r_{ini},\ r_{\tau=\tau_f} = r_{term} \tag{23}$$

$$\frac{dr}{d\tau}_{\tau=0} = \dot{r}_{ini},\ \frac{dr}{d\tau}_{\tau=\tau_f} = \dot{r}_{term}$$

$$\frac{d^2r}{d\tau^2}_{\tau=0} = \ddot{r}_{ini}$$

where τ_f denotes end condition of non-dimensional time τ, $\beta_{ini}, \dot{\beta}_{ini}, \varepsilon_{ini}, \dot{\varepsilon}_{ini}, r_{ini}, \dot{r}_{ini}$ denote initial conditions of a boosting section that are obtained from navigation solution, $\beta_{term}, \dot{\beta}_{term}, \varepsilon_{term}, \dot{\varepsilon}_{term}, r_{term}, \dot{r}_{term}$ denote end conditions of a boosting section that are predetermined according to the design result of nominal trajectory, $\ddot{\beta}_{ini}, \ddot{\beta}_{term}, \ddot{r}_{ini}$ denote boundary conditions of second derivatives. According to Eqs. (21-23), all polynomial coefficients and τ_f is calculated by solving simultaneous equations.

First and second derivatives of Eq. (17) derive following mathematical relations.

$$\frac{dt}{d\tau} = \alpha + \tau\frac{d\alpha}{d\tau} \tag{24}$$

$$\frac{dD}{d\tau} = -\left(2\frac{d\alpha}{d\tau} + \tau\frac{d^2\alpha}{d\tau^2}\right)D^2, \tag{25}$$

$$D = \left(\alpha + \tau\frac{d\alpha}{d\tau}\right)^{-1}$$

where D denotes intermediate variable. Considering the condition that $F_\beta, F_\varepsilon, F_r$ are the components of control force F, following condition is derived according to Eqs. (14-16).

$$\left(r\,\ddot{\beta} + 2\dot{r}\dot{\beta}\right)^2 + (r\ddot{\varepsilon} + 2\dot{r}\dot{\varepsilon})^2 \tag{26}$$
$$+\left(\ddot{r} - r\left(\dot{\beta}^2 + \dot{\varepsilon}^2\right) + \frac{\mu_{moon}}{r^2}\right)^2 = (F/m)^2$$

By solving Eqs. (24-26) in terms of second derivatives of α wrt. τ a quadratic equation is obtained as follows.

$$P_2\left(\frac{d^2\alpha}{d\tau^2}\right)^2 + P_1\frac{d^2\alpha}{d\tau^2} + P_0 - (F/m)^2 = 0 \tag{27}$$

$$P_0, P_1, P_2 \text{ : Function of } \alpha \text{ and } \frac{d\alpha}{d\tau}$$

where P_0, P_1, P_2 denotes coefficients of the quadratic equation. Solution of Eq. (27) derives second order differential equation in terms of α wrt. τ.

Non-dimensional time series of α is calculated according to numerical integration of the second order differential equation. By substituting α and its first derivative for Eqs. (18-20) and their derivatives, actual time series of reference trajectory is obtained. Required control force F is also obtained by substituting actual reference trajectory states for Eq. (26). Total mass of the spacecraft m is also updated according to F by

solving rocket equation.

4.3. Evaluation of guidance solution

Proposed guidance logic is tested by simulation. Nominal trajectory is as derived in previous section. Lunar gravity field model 'jggrx_0900d' that is based on NASA's GRAIL observation data is applied. [8] The order of spherical harmonics of the gravity field model is reduced to 100×100. The objective of simulation test is to confirm the guidance logic reproduces nominal trajectory and corresponding control input. Therefore, navigation error is not applied in this simulation. Disturbance due to gravitational field model or control latency is compensated by flight path tracking logic that is incorporated in the simulator.

Guidance logic is evaluated by comparing end condition of guidance solution and nominal trajectory in boosting section #3. Guidance solution that is expressed in terms of β, ε, r is transformed into $DR, CR, h, v_\beta, v_\varepsilon, v_r$ for evaluation purpose according to following transform equations.

$$\begin{bmatrix} DR \\ CR \\ h \end{bmatrix} = \begin{bmatrix} \beta R_{moon} \\ r \sin \varepsilon \\ r \cos \varepsilon - R_{moon} \end{bmatrix} \tag{28}$$

$$\begin{bmatrix} v_\beta \\ v_\varepsilon \\ v_r \end{bmatrix} = \begin{bmatrix} \dot{\beta} r \cos \varepsilon \\ \dot{r} \sin \varepsilon + r\dot{\varepsilon} \cos \varepsilon \\ \dot{r} \cos \varepsilon - r\dot{\varepsilon} \sin \varepsilon \end{bmatrix} \tag{29}$$

End conditions of boosting#3 are evaluated as shown in Table 6. Trajectory states of guidance solution at the end of boosting#3 agrees to those of nominal trajectory. Duration of boosting sections have slight difference that affects end condition of total mass of the spacecraft. Comparison of trajectory shape, time series of velocities, and time series of control input are shown in Figs. 12-16. It is confirmed that the guidance logic properly reproduces nominal trajectory states.

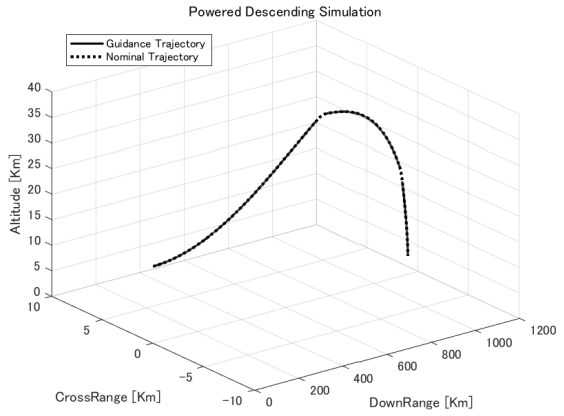

Fig. 12. Comparison of guidance solution and nominal trajectory (Trajectory Shape).

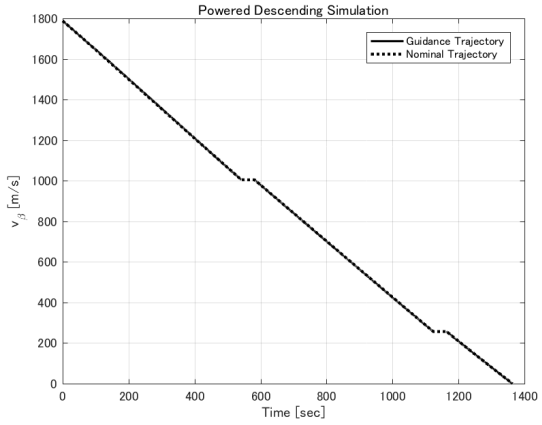

Fig. 13. Comparison of guidance solution and nominal trajectory (Time series of horizontal velocity).

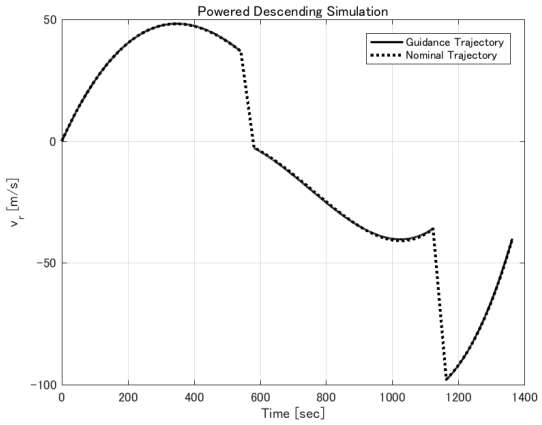

Fig. 14. Comparison of guidance solution and nominal trajectory (Time series of vertical velocity).

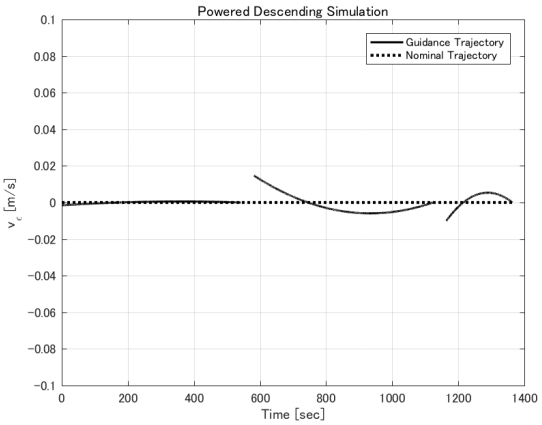

Fig. 15. Comparison of guidance solution and nominal trajectory (Time series of out-of-plane velocity).

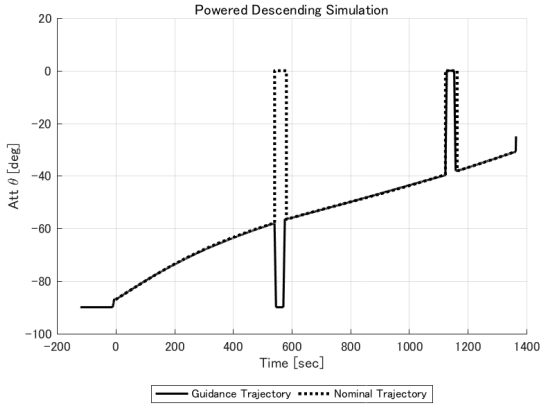

Fig. 16. Comparison of guidance solution and nominal trajectory (Time series of control input, attitude pitch).

Table 6. Evaluation by comparing boosting#3 end conditions.

Items	Unit	Guidance	Nominal
End condition (DR)	km	1156.76	1156.76
End condition (CR)	km	0.00	0.00
End condition (h)	km	3.50	3.50
End condition (v_β)	m/s	0.00	0.00
End condition (v_ε)	m/s	0.00	0.00
End condition (v_r)	m/s	−40.00	−40.00
Duration of boosting#1 (T_{b1})	s	541.23	541.84
Duration of boosting#2 (T_{b2})	s	541.87	541.84
Duration of boosting#3 (T_{b3})	s	199.81	200.00
Total mass of spacecraft (m)	kg	186.62	185.00

5. Robustness Verification of the Guidance Logic

5.1. Analysis model definition

This section introduces analysis to verify robustness of the guidance logic. The analysis is performed by means of montecarlo simulation. The guidance logic targets end states of each boosting section of nominal trajectory according to initial states of respective boosting section that are estimated by navigation solution. To verify robustness of the guidance logic, deviation of estimated states from nominal trajectory that is incurred by IMU accumulated navigation error and navigation error due to vision based navigation must be considered.

Figure 17 shows conceptual explanation of the analysis model. By orbital maneuver in lunar circular orbit, the spacecraft is injected into states where powered descending is planned to initiate. Injection error due to maneuver control accuracy or related navigation accuracy is applied as actual trajectory deviation. For targeting of the first boosting section, vision based navigation is applied, therefore its navigation accuracy must be considered as a source of deviation. Once boosting section initiated, the spacecraft controls its trajectory according to the flight path tracking control logic, therefore accumulated IMU navigation error must be considered as a source of deviation. In the analysis model, vision based navigation error is applied at the beginning of boosting section, and accumulated IMU navigation error is applied at the end of boosting section for simplification purpose. After completion of the first boosting section, actual states that consider accumulated IMU navigation error are calculated, then they are propagated during the first coasting section. The same procedure is repeated for the second or the third boosting sections. Finally, end states of the third boosting section are evaluated in terms of guidance accuracy.

5.2. Analysis example

A montecarlo simulation is performed as an example of robustness verification analysis. The error sources those are applied as analysis condition are as shown in Table 7. All error sources are noise type error and they are expressed in terms of 3σ value of normal distribution.

Table 7. Error source examples for robustness verification analysis.

3σ error sources	Unit	$[\beta, \varepsilon, r]$
Initial actual position deviation	km	[1,1,1]
Initial actual velocity deviation	m/s	[5,5,5]
Vision based navigation position error	km	[0.45, 0.45, 0.45]
Vision based navigation velocity error	m/s	[1.5,1.5,1.5]
IMU accumulated navigation error		
Boosting section#1 position error	km	[2.4, 2.4, 2.4]
Boosting section#1 velocity error	m/s	[6,6,6]
Boosting section#2 position error	km	[1.2, 1.2, 1.2]
Boosting section#2 velocity error	m/s	[3,3,3]
Boosting section#3 position error	km	[0.6, 0.6, 0.6]
Boosting section#3 velocity error	m/s	[1.5,1.5,1.5]

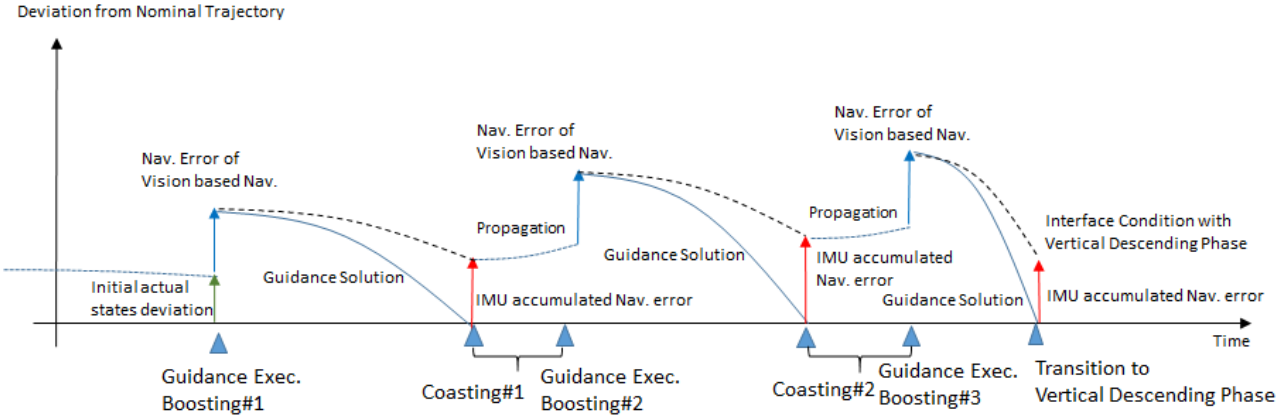

Fig. 17. Conceptual explanation of the analysis model for robustness verification of the guidance logic.

1000 case montecarlo simulation is performed. Evaluation result of guidance accuracy at the end of the third boosting section is shown in Table 8. Distribution of trajectory shape, time series of velocity distribution, and time series of control input distribution are shown in Figs. 18-22. It is confirmed that the guidance logic properly generates guidance trajectories according to initial condition of each boosting section. It is identified that end condition of crossrange (CR) and vertical velocity (v_r) have relatively large 3σ distributions.

As for crossrange distribution, it is caused by the difference of timing of guidance completion. Duration of boosting sections can vary according to guidance solution that leads to variation of total guidance time. Evaluation is performed in terms of relative states wrt. landing target point, therefore arrival time difference in combined with moon rotation affects crossrange distribution. Relation of arrival time difference and crossrange deviation at guidance end condition is shown in Fig. 23. The figure clearly indicates that arrival time difference and crossrange deviation have linear relation.

As for vertical velocity distribution, it is caused by the feature of the guidance logic. As formulated in previous section, the guidance logic utilizes non-dimensional coefficient α. This coefficient works as expansion or contraction of time in case sufficient trajectory control force is not provided due to limitations of configuration of the spacecraft. Figure 24 shows distribution of trajectory control force. In some cases, control force is saturated at upper or lower limit, that leads to increase or decrease of α. Ideal solution has $\alpha = 1$ for whole time series. When $\alpha \neq 1$ at the end of boosting section, guidance velocities have error according to transformation process from non-dimensional velocities those agree to boundary conditions. This indicates that upper or lower limit of trajectory control force variation affects guidance velocities; therefore, guidance parameters must be adjusted considering performances of propulsion system.

It is concluded that proposed autonomous guidance logic has sufficient robustness according to the result of montecarlo simulation. It is also identified that the guidance logic has a feature that must be considered in determination process of interface condition between powered descending phase and following vertical descending phase.

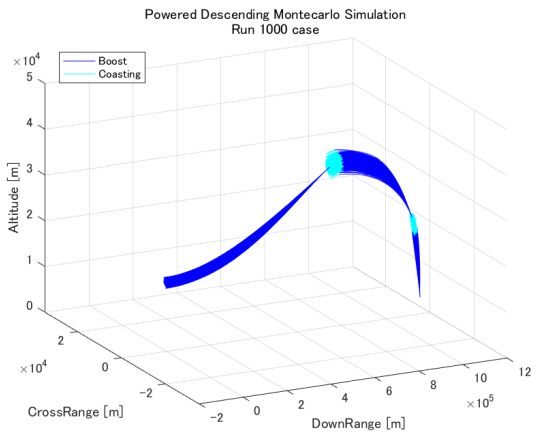

Fig. 18. Distribution of guidance trajectory shape.

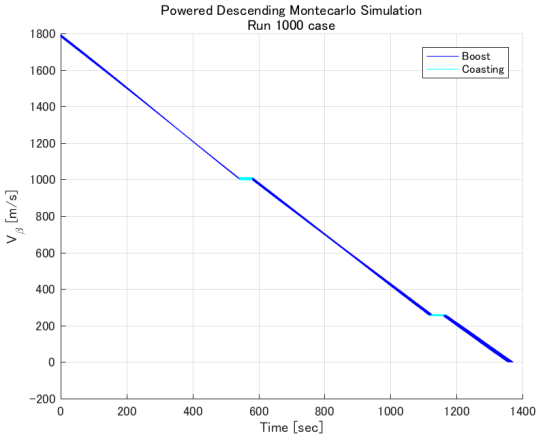

Fig. 19. Distribution of time series of horizontal velocity.

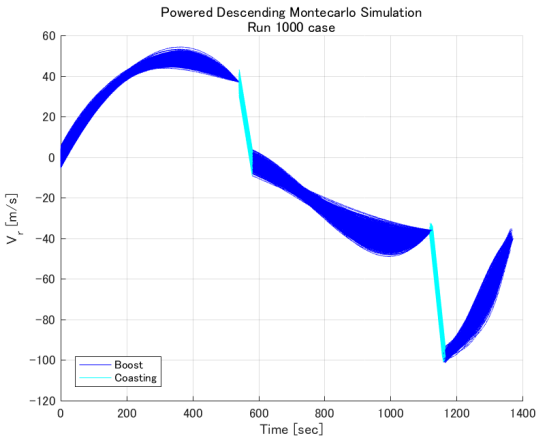

Fig. 20. Distribution of time series of vertical velocity.

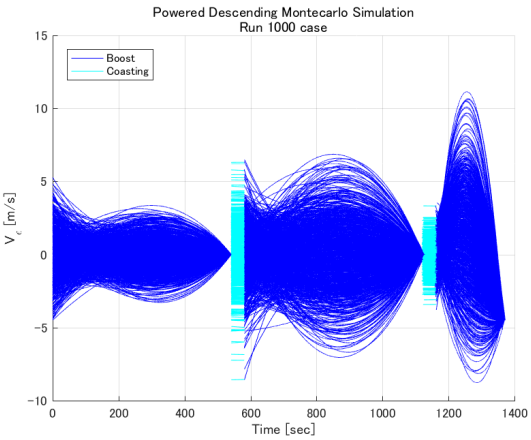

Fig. 21. Distribution of time series of out-of-plane velocity.

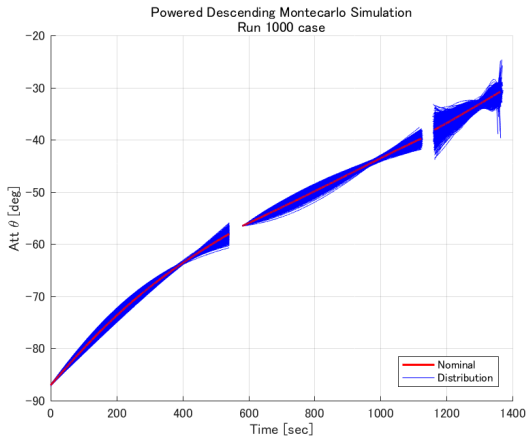

Fig. 22. Distribution of time series of control input, attitude pitch.

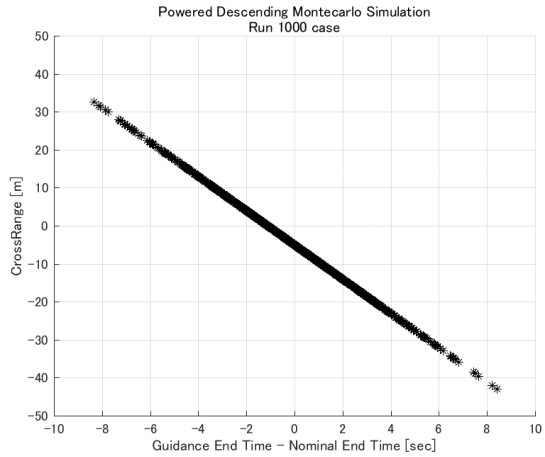

Fig. 23. Relation of arrival time difference and crossrange deviation at guidance end condition.

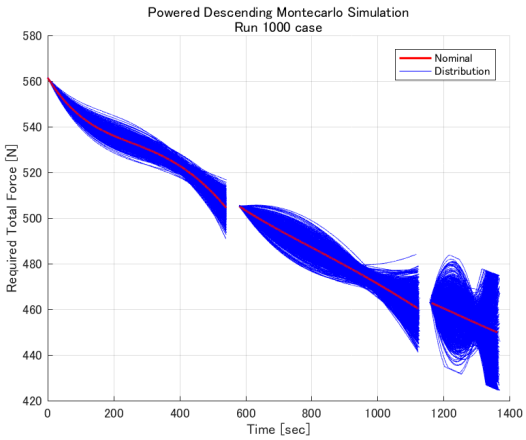

Fig. 24. Distribution of trajectory control force (saturations occur during the third boosting section).

Table 8. Evaluation of end condition of guidance solution wrt. landing target point according to 1000 case montecarlo simulation.

Relative states wrt. landing point	Unit	Mean	3σ
Downrange (DR)	m	-2.1	0.0
Crossrange (CR)	m	-4.0	38.5
Altitude (h)	m	3500.0	0.0
Horizontal velocity (v_β)	m/s	0.00	0.00
Out-of-plane velocity (v_ε)	m/s	0.00	0.23
Vertical velocity (v_r)	m/s	-40.00	2.02

6. Conclusion

This study focuses on autonomous guidance logic for precise lunar landing. First, an optimal nominal trajectory in terms of minimum fuel consumption is derived according to trajectory optimization technique. Second, autonomous guidance logic is formulated and it is tested to confirm that it reproduces nominal trajectory and corresponding control input. Third, analysis is performed by means of montecarlo simulation to verify robustness of the guidance logic. It is confirmed that the guidance logic properly generates guidance trajectories according to initial condition of each boosting section. This study concludes that proposed autonomous guidance logic has sufficient robustness. This study also identified the feature of the guidance logic that must be considered in determination process of interface condition between powered descending phase and following vertical descending phase.

Acknowledgments

We thank S. Ueno and T. Higuchi for technical advices.

References

1) Kawasaki, M.: *Study on Polynomial Guidance Law for the Smart Lander for Investigating Moon*, Proceedings of ISTS 28th, 2011.
2) Aoki, H., Yasumitsu, R., Kunugi, M., Takeya, A., Takatsuka, N., Yoshikawa, S. and Fujii, Y.: *A Study on Guidance, Navigation and Control about SLIM*, Proceedings of ISTS 28th, 2011.
3) Sawai, S., Mizuno, T., Fukuda, S., Nakaya, K., Haruyama, J., Okada, T., Nakatsuka, J., Saiki, T., Yasumitsu, R. and Morishima, K.: *Conceptual Study on SLIM*, Proceedings of ISTS 28th, 2011.
4) Ueno, S., Itagaki, H. and Yamaguchi, Y.: *Near-minimum Fuel Guidance and Control System For a Lunar Landing Module*, Proceedings of ISTS 21st, 1998.
5) Ueno, S. and Yamaguchi, Y.: *3-Dimensional Near-Minimum Fuel Guidance Law of a Lunar Landing Module*, Proceedings of AIAA Guidance, Navigation, and Control Conference and Exhibit, 1999.
6) Takino, T., Nomura, I., Moribe, M., Kamata, H., Takadama, K., Fukuda, S., Sawai, S. and Sakai, S.: *Crater Detection Method using Principal Component Analysis and its Evaluation*, Proceedings of ISTS 30th, 2015.
7) Usui, K., Harada, T., Takadama, K., Kamada, H., Fukuda, S., Sawai, S. and Sakai, S.: *Adjusting SLIM Spacecraft Location Estimation to Crater Detection for High Precision and Computational Time Reduction*, Proceedings of ISTS 30th, 2015.
8) The Geosciences Node of NASA's Planetary Data System (PDS), http://pds-geosciences.wustl.edu/ (accessed December 3, 2015).